2018

Time-Evolved Constant Voltage Conductivity Polymeric Materials

Brian Wood
Utah State University

JR Dennison
Utah State Univesity

David King
Utah State University

Time-Evolved Constant Voltage Conductivity Measurements of Common Spaceborne Polymeric Materials

Brian Wood, David King, and JR Dennison

***Abstract*—Long-duration conductivity measurements were made for low density polyethylene (LDPE), polyimide (PI), polyether ether ketone (PEEK), and biaxially-oriented polypropylene (BOPP) to determine their bulk conductivity near room temperature as a function of time. These common thin-film spacecraft material samples were vacuum baked to remove moisture and volatile contaminants to better simulate space conditions. The constant voltage conductivity (CVC) method used a very stable, low-noise DC voltage source and measured the resulting current in a parallel plate geometry. Due to the extremely low conductivity of these four polymeric materials, extended experiments of up to 10 days were necessary to establish equilibrium current flow and determine dark conductivity. The lower instrumental limit of conductivity measurements with this setup is $\lesssim 2 \cdot 10^{-21}\ (\Omega \cdot cm)^{-1}$. Changes in conductivity due to field-enhanced conductivity and radiation induced conductivity as well as varying voltages, temperatures and dose rates are also considered.**

Data for each material are fit to a multi-term model to account for the different conduction mechanisms within highly disordered insulating materials (HDIM), including polarization, dispersive transport, and dark conductivity. The regimes of disorder-induced dispersive transport demarcated by the transit time are observed in all materials, indicative of hopping transport between trap states in HDIM. Information on the energy distribution of localized trap states responsible for electron conduction in HDIM is extracted from the fitting parameters. Magnitudes and time-dependence of conductivity are reported, along with estimated polarization, transit, equilibrium, and decay times; these are compared favorably with previous measurements using constant voltage and charge storage decay conductivity methods. These fits can be used with model simulations of time-dependent spacecraft charging to determine non-equilibrium transient conductivity for specific applications.

***Index Terms*— Conductivity, Constant Voltage Conductivity, Disordered Materials, Electron Transport, Polymers, Resistivity, Temperature Assisted Hopping, Variable Range Hopping.**

I. Introduction

Charging effects on spacecraft have been extensively documented and researched in an attempt to prevent critical failure of key spacecraft components [1,2]. Charge exchange between the craft and its radiation environment and charge transport within spacecraft materials pose a complex problem on both macroscopic [1] and microscopic [3,4] scales. These traits of charge accumulation, dissipation and transport are characterized by material properties including conductivity, radiation induced conductivity, permittivity, electrostatic breakdown, electron emission, and cathodoluminescence [2].

Thin film and bulk polymeric highly disordered insulating materials (HDIM), such as the four materials studied here, are ubiquitous in spacecraft. These materials inhibit charge transport very well, and therefore can appreciably store charge due to their long decay time and create charge imbalances that can lead to deleterious electrostatic discharge (ESD) events [1,2,5]. Determining accurate values for conductivity, particularly equilibrium dark current conductivity (σ_{DC}), of these materials is essential to calculate and model internal charge storage and movement on spacecraft [6,7]. However, the same extremely slow transport and long equilibration times that enhances charge accumulation making the study of these materials critical, also makes their measurements a challenge [4,8,9]. The extreme disorder of HDIM also makes their underlying materials physics both unique and complex [3]. Thus, understanding the temporal evolution of measurements under applied field and the underlying transport mechanisms of HDIM due to the extreme insulating properties and highly disordered structure of these materials, has proven difficult.

The focus of this study is the time evolution of conductivity as measured with the Constant Voltage Conductivity (CVC) test method. This study builds on previous work focused on the measurement, experimental uncertainties, modeling and underlying physics after samples have come to equilibrium in these measurements [8,9]. Section II provides a brief review of relevant transport theory for HDIM. A model for the time-dependent conductivity incorporating polarization, dispersive transport, and equilibrium conductivity is introduced, and the relative importance of the different conduction mechanisms on different times scales is discussed. Sections III and IV present experimental details and discuss experimental and systematic uncertainties, including those due to non-equilibrium voltages, temperatures and dose rates. Section V reports long-duration measurements and comparison of the magnitudes and time-

Brian Wood and JR Dennison are with the Materials Physics Group at Utah State University (USU), Logan, UT 84325-4415 USA (emails: brian.wood314@gmail.com and jr.dennison@usu.edu). David King was an undergraduate physics major at USU and is now a PhD student in physics at University of Wyoming. (email: davidking.ian@gmail.com). This study was partially supported by an Undergraduate Research and Creative Opportunities (URCO) grant from the USU Office of Research and Graduate Studies.

dependence of conductivity for four polymeric materials with the model.

II. THEORY

Understanding the electrical conduction of very good insulators—both very wide bandgap insulators and HDIM—cannot be directly understood in terms of familiar band structure concepts used for crystalline semiconductor materials. Through the quantum mechanical treatment of the long-range order of crystalline semiconductors, conduction by promotion of charge carriers across well-defined band gaps has come to be the welcomed conceptual norm for explaining electron transport.

However, the distinction between extended states resulting from long-range order, and spatially localized trap states resulting from disorder found at energies within the bandgap is a defining feature of charge transport in amorphous solids and HDIM. For HDIM, the density of states (DOS) of such disordered localized states has its energy distribution characterized by a width parameter α [3,4,10]. Conduction is described in terms of discrete transitions between spatially localized states through tunneling hopping mechanisms, such as thermally-assisted hopping and nearest-neighbor (or variable-range) hopping [4,10]. One can characterize conduction in terms of the time it takes charge to traverse a material via hopping. For transport involving only a single trap state energy (*i.e.* $\alpha \to 0$), charge motion in a parallel plate geometry is a diffusive process with time dependence of t^{-1} and characterized by a transit time $\tau_{transit}$, the time for a charge front to move across a sample [3]. In HDIM there is a distribution of times for charge carriers to move from one trap to the next and across the sample, as carriers have longer retention times in more tightly bound trap states. Therefore, the injected internal charge distribution expands across an HDIM sample, with the majority of the charge density staying near its origin. There is a displacement current contribution to measured current as the charge distribution is modified, even before charge has moved across the full width of the sample.

This leads to conductivity behavior unique to HDIM that results from hopping between localized defect trap states with a distribution of energies. This was first explained by Scher and Montroll [11] for charge transport across disordered semiconductors, and later extended to HDIM, as

$$I(t) = \begin{cases} I_0 t^{-(1-\alpha)}\,\Theta(\tau_{trans} - t), & \text{for } t < t_{transit} \\ I_0 t^{-(1+\alpha)}\,\Theta(t - \tau_{trans}), & \text{for } t > t_{transit} \end{cases}. \quad (1)$$

The first term, dispersive transport, models times before the leading edge of the charge front reaches the rear electrode at $\tau_{transit}$, and the second term describes transitive transport for times after $\tau_{transit}$. The Heaviside function, $\Theta(t)$, is used to separate these terms temporally. α is a parameter that describes the distribution width of the localized DOS, where $0 \le \alpha \le 1$ [3]. Weak disorder leads to narrow distributions of defect state energies, and dispersive and transitive transport merge to diffusive transport in the limit $\alpha \to 0$. α is an intrinsic property of a material and can only be changed by modifying the distribution of states, for example by chemical modifications, mechanical deformation, or a total incident radiation dose.

Charge transport in the parallel plate configuration is modeled macroscopically from Ohm's law in terms of the conductivity as

$$\sigma(t) \equiv \vec{\boldsymbol{J}}(t)/\vec{\boldsymbol{E}}(t) = [I(t) \cdot d]/[V(t) \cdot A]\,, \quad (2)$$

where $I(t)$ and $V(t)$ are the measured time-dependent current and applied voltage, and d and A are the time-independent sample thickness and electrode area, respectively.

The total conductivity has been previously modeled for a variety of applications with time-dependent macroscopic models for a number of conduction mechanisms that includes polarization, dispersive transport, dark current conductivity, radiation induced conductivity, AC conductivity, and displacement currents resulting from time-dependent changes in applied voltage and permittivity (see more detailed treatment in Appendix B of ref. [8]). For the CVC method it is shown that the conductivity can be expressed as [8]

$$\sigma(t) = \sigma_P^0 e^{\frac{-t}{\tau_P}} + \left\{\sigma_{disp}^0 t^{-(1-\alpha)}\Theta(\tau_{transit} - t) + \sigma_{trans}^0 t^{-(1+\alpha)}\Theta(t - \tau_{transit})\right\} + \sigma_{DC}\,. \quad (3)$$

The initial term in Eq. (3) is a polarization displacement current, which results from the response of the internal charge of the material to the applied electric field, essentially a time-dependent permittivity $\varepsilon_r(t)$. For many materials, this exponential decay dominates the conductivity for short time periods, until the material has mostly responded to the applied field. This idealized relaxation model is characterized by a polarization time constant, τ_P. Relatively short time constants for electronic, atomic, molecular and interfacial responses can range from the very fast—well below time scales measured in typical CVC tests—to perhaps 10^2 s to 10^3 s. Measurements will often exhibit more than one time constant and amplitude associated with different response mechanisms.

For longer time scales, the conductivity is dominated by the dispersive displacement current, *i.e.* the components of Eq. (1) discussed above. Both terms fall off as power laws of time; the dispersive term at shorter time with a smaller time constant (1-α), and the transit term at longer time with a larger time constant (1+α). The signature of the transition at $\tau_{transit}$ is most evident in a log-log plot of current versus time, where both terms are linear and there is a distinct change in slope at $\tau_{transit}$, as the transport mechanism shifts from the dispersive to the transitive regime. If the Scher and Montroll model is applicable, the fitting parameter α is the same for the dispersive and transitive terms, that is the sum of the slopes before and after $\tau_{transit}$ is [(1-α) + (1+α)]=2. For disordered semiconductors $\tau_{transit}$ is in the range of 10^{-6} s to 10^{-1} s [3,11], while for HDIM $\tau_{transit}$ can range from 10^1 s to 10^5 s as trap state energies and disorder increase.

The final term, σ_{DC} or dark conductivity, is the equilibrium time-independent conductivity of electron transport across the material reached after long time spans as the charge distribution within the material becomes uniform and the change in the dispersive displacement current become negligible. One time scale related to σ_{DC} is the time to equilibrium, τ_{eq}; this can be difficult to accurately identify if the dark current is very small

or there are other contributions—discussed in Sec. IV—that cause changes in the dark current. From an operational point of view, τ_{eq} is defined here as when the contribution from the transitive current becomes smaller than the noise in the dark current, $\sigma_{transit}(\tau_{eq}) = \Delta\sigma_{DC}$.

Another related time scale is the decay time, $\tau_{decay} \equiv (\epsilon_o\epsilon_r / \sigma_{DC})$, for a charge layer deposited on a surface to discharge to 1/e of the initial charge; it is simply the intrinsic form of the RC time constant of a discharging capacitor and is what is measured in charge storage (or surface voltage decay) conductivity (CSC) experiments to determine σ_{DC}. One could expect that $\tau_{eq} < \tau_{decay}$, since the electric field driving charge is maintained for CVC experiments while the electric field diminishes as charge is dissipated in CSC measurements. For a relative permittivity of ϵ_r=3 (typical for polymers), τ_{decay} varies from 10^4 s (~3 hr) to 10^8 s (~4 yr) for conductivities of $\sim 3x10^{-17}(\Omega \cdot cm)^{-1}$ to $\sim 2x10^{-21}(\Omega \cdot cm)^{-1}$, respectively.

The various time scales outlined above can be arranged in an expected order of increasing times as

$$\tau_Q < \tau_p < \tau_{transit} < \tau_{eq} < \tau_{exp} < \tau_{decay} \ . \quad (4)$$

The time scales related to the conduction mechanisms— τ_p, $\tau_{transit}$, $\tau_{decay,}$ and τ_{eq} , are bracketed here with two experimental time scales. τ_{exp} is simply the duration of the CVC measurements, which in an ideal experiment, always exceeds the time to equilibrium τ_{eq}. τ_Q is the time to establish the initial charge (voltage) on the electrodes; this includes contributions from the voltage supply response time and the charge injection process [8]. Typically, $\tau_Q \lesssim 0.2$ s ($\tau_Q \lesssim 10^{-2}$ s for the battery voltage supply used here) and is therefore not evident in the data shown here.

III. Experimental Setup

A schematic of the Constant Voltage Conductivity (CVC) test apparatus [8] is shown in Fig. 1, illustrating the electrical and computer interface connections and the configuration with samples sandwiched between two parallel plate electrodes. Sample current, applied voltage, and temperature data are recorded by a custom *LabView*™ program through a computer interface. Currents and voltages are recorded at ~ 3 s intervals, except during the initial minutes of each experiment where ≲1 s interval can be used. Temperature is recorded at ~10 s intervals.

An aluminum plate serves as the front high-voltage electrode on which samples are mounted. A highly-polished (1.98±0.02 cm^2) copper guarded rear electrode held near ground is used to monitor the sample current. The test fixture clamps the electrodes to the sample with calibrated springs that provide ~300 kPa pressure, in compliance with the ASTM D257 standard [12]. This entire assembly is housed in a high vacuum chamber with a base pressure of $< 10^{-5}$ Pa.

Sample current is measured with a relatively slow, sensitive electrometer (Keithley model 616) with ~1 fA current sensitivity. A battery powered high voltage source consisting of 9 V rechargeable NiMH batteries in series is used to eliminate any AC contributions to measured current [13]. Potentials up to 800 V were achieved with ~90 batteries in series. Variation

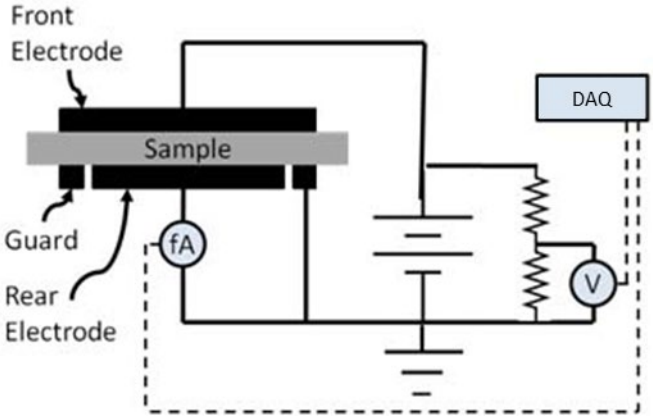

Fig. 1: Schematic of Constant Voltage Conductivity (CVC) experimental setup, showing the parallel plate configuration, along with the current and voltage signals recorded via a computer interface. Thermocouple sensors (not shown) record temperatures of the front and rear guard electrodes, along with chamber temperature and room ambient [8].

in accuracy of the applied voltage (due primarily to long-term drift) are directly monitored and compensated for in the conductivity calculations; therefore, they do not contribute any inaccuracy to the conductivity. Over typical experiments of 10 days (10^6 s), the battery supply discharges <0.5% at a rate of ~7 mV/hr. Voltage is monitored during experiments with 0.03 V (<40 ppm) resolution using a 100:1 voltage divider in parallel with the sample recorded with a 16-bit DAQ card. Further details are given in ref. [8].

All measurements for this study were taken near room temperature; this was found to fluctuate by about ±0.5 K over fairly repeatable daily cycles. Temperatures were monitored with Type K thermocouples (~0.5 K accuracy and ~0.001 K precision) mounted in the front electrode, rear guard electrode, chamber wall, and room ambient. Temperature gradients across the sample were on the order of 1 K. Although not used for these studies, temperature management is available using PID controllers with resistive heaters (up to ~400 K) or a heat exchanger connected to a flow chiller (Julabo Model Presto-W85; ~230 K to ~370 K) or a liquid nitrogen source (down to ~120 K). These will be used in future studies of temperature-dependent conductivity.

Once samples were prepared and mounted in the CVC chamber at vacuum, experimental runs commenced. Background currents with grounded samples were recorded for prolonged periods at the beginning and end of each run, so that linear drift in any small instrumentation offset current could be subtracted from the measured data. Runs lasted until the samples reached current equilibrium, which took up to tens of days. Once equilibrium was reached, the voltage source was shut off and the discharge current versus time was recorded. Using measured values for the time-independent sample thicknesses and electrode area, the time-dependent conductivity was then determined with Eq. (3) and modeled with Eq. (4).

Well-characterized, high-uniformity polymer samples from Goodfellow were used for all tests.

- Low density polyethylene (LDPE) samples (ASTM D-5213 type I [14]) tested had measured thicknesses of 27.4 μm ±0.7%, density of 0.92±0.01 g/cm^3 [15], estimated

crystallinity of 50% [16], a peak fractional mass distribution of ~$6{\cdot}10^3$ amu [9, 18], and ε_r=2.27±0.08 [15]. Measurements were made at 420 V, or ~ 17 MV/m

- Polyimide (PI) samples of Kapton HN™ (ASTM D-5213 type I [14]) had measured thicknesses of 25.0 μm ±2%, density of 1.43±0.01 g/cm^3 [19], and ε_r=3.5±0.1 [19]. Measurements were made at 800 V, or ~ 32 MV/m.
- PEEK samples had measured thicknesses of 29.6 μm ±1%, density of 1.26±0.005 g/cm^3, and ε_r=3.25±0.05 [20]. Measurements were made at 800 V, or ~ 32 MV/m.
- Biaxially oriented polypropylene (BOPP) samples tested had measured thicknesses of 27.6 μm ±1%, density of 0.90±0.05 g/cm^3 [21], and ε_r=2.4±0.2 [21]. Measurements were made at 800 V, or ~ 32 MV/m.

All samples were chemically cleaned with methanol prior to a bake out at ~385±5 K (338±3 K for LDPE, as the melting point for LDPE lies around 383 K) under <10^{-3} Pa vacuum for ≳4 days while in contact with a grounded surface, to eliminate absorbed water and volatile contaminants and any residual stored charge [9]. After bake out, samples were mounted on voltage plates and stored in a dry nitrogen environment until ready for measurements.

Nominal dark current conductivity for unbaked samples using standard ASTM 257 test methods [12] and breakdown field strengths for unbaked samples using standard ASTM 149 test methods [24] were listed as ~$8x10^{-17}$ $(\Omega \cdot cm)^{-1}$ and 200 MV/m for LDPE [16], ~$1x10^{-18}$ $(\Omega \cdot cm)^{-1}$and 303 MV/m for PI [19], ~$2x10^{-16}$ $(\Omega \cdot cm)^{-1}$ and 200 MV/m for PEEK [20], and ~$1x10^{-17}$ $(\Omega \cdot cm)^{-1}$, and 110-150 MV/m for BOPP [21], respectively. The nominal breakdown voltages as determined by a 2-parameter Weibull fit for vacuum baked samples were measured as 316 MV/m for LDPE, 272 MV/m for PI, 200 MV/m for PEEK, and 337 MV/m for BOPP, respectively [22].

IV. Experimental Uncertainties

Instrumental limits on the precision and accuracy of measured conductivity associated with the four measured quantities in Eq. (3) are set by a number of factors. Uncertainty in lower conductivities is dominated by the precision in the current measurements of ~1 fA [8]. This corresponds to a resolution limit of measured conductivity of $\Delta\sigma_{res} = 2x10^{-21}$ $(\Omega \cdot cm)^{-1}$for typical values of V, d and A. When samples reach equilibrium currents, signal averaging of measurements over 10^3 s can typically reduce the precision to ~1×10^{-16} A and $\Delta\sigma_{res} = 2x10^{-22}$ $(\Omega \cdot cm)^{-1}$; such signal averaging is only valid if conductivity has reached equilibrium and fluctuations in measured currents and voltages are small and largely uncorrelated in time.

Values for d and A are the time-independent and therefore only contribute to the accuracy of the measurements [8]. Uncertainties in current dominate at lowest conductivities; however, at conductivities $> 10^{-19}$ $(\Omega \cdot cm)^{-1}$ typical accuracies for sample thickness of 1% to 2% can limit the accuracy in conductivity.

The applied electric field can affect σ_{DC} through a field-enhanced conductivity, which only becomes more than a ~10% effect at applied fields >10% of the electrostatic breakdown field [9,16]. Field-induced enhancements at ~20% of the breakdown field strength were found to be about a factor of 2 for similar LDPE samples [9], consistent with Poole-Frenkle theory of field-enhanced conductivity [23]. Thus, measurements here performed at ≲32 MV/m (~5%, 12%, 16% and 10% of the electrostatic breakdown field for LDPE, PI, PEEK and BOPP, respectively) may introduce a small constant increase in conductivity; however, since the drift in this applied field is small, this will produce only a small shift in accuracy and will not affect precision.

Fluctuations in voltage can directly affect the free electron charge transport current and the corresponding conductivity through Eq. (3). More importantly, even very small magnitude short-term voltage fluctuations can produce displacement currents proportional to dV/dt which are comparable to the dark current. Even low-noise AC-to-DC power supplies have 60 Hz and higher frequency ripples that produce larger displacement currents [8]. A battery powered high voltage source is used here to minimize such short-term fluctuations in voltage [13]. The voltage fluctuations for the battery voltage supply used occur on time scales on the order of <10^2 s and deviate no more than 80 ppm, making these effects on precision much less than current-dependent uncertaities. Further, since conductivity determinations include voltage measurements at each time step, slow-scale voltage decay which does not produce significant displacement current does not affect uncertainty in conductivity. Hence, voltage measurements do not contribute significantly to the accuracy of conductivity measurements.

Contributions to precision and accuracy due to non-equilibrium temperatures, voltages, and dose rates are also considered here. Changes in the temperature, ΔT, can manifest in several ways. Changes in sample temperature cause direct changes in the dark conductivity, $\sigma_{\Delta T} \equiv \left[\frac{d\sigma_{DC}(T)}{dT}\right] \cdot \Delta T$ (and, presumably, similarly for the polarization and transient conductivities). This is clearly seen in the LDPE, PI, PEEK and BOPP conductivity data, as discussed in Sec. V, and is attributed to the small daily cyclic changes in room temperature. On a microscopic scale, thermal shot (Johnson) noise is produced by random motion of the constituent particles; this contribution to the threshold for lowest measurable conductivity is on the order of ~$2x10^{-23}(\Omega \cdot cm)^{-1}$ for LDPE measurements made at room temperature under 420 V [8].

Changes in voltage are largely considered above. Figure 2(b) shows a graph of voltage and temperature versus time for long times. Measured voltage fluctuations of the battery supply due to diurnal temperature fluctuations in the lab are on the order of ±75 mV or ±100 ppm at ~300 mV/K. Thus, the influence of a resulting displacement current from a typical half day temperature rise or fall ±0.3 K on the order of 7 μV/s are negligible.

Changing dose rate can cause well-known time-dependence in radiation induced conductivity (RIC); this includes onset RIC for increasing dose rates and delayed RIC for decreasing dose rates [4,16,24]. The CVC apparatus has neither artificially applied or time-varying dose rates. However, even in a situation with no applied dose, RIC can contribute to the threshold for lowest measurable conductivity [8]. The small amount of energy deposited in samples from the ubiquitous (and largely un-shieldable) constant background dose from very high energy cosmic radiation at sea level is ~0.26 mGy/yr [25], which

produces a background conductivity on the order of $\sim 3x10^{-23}(\Omega \cdot cm)^{-1}$ for LDPE samples and measurement methods considered here [8].

V. Results and Analysis

Conductivity data as a function of time for LDPE, PI, PEEK, and BOPP are shown in Figs. 3, 4, 5, and 6, respectively. These plots also show the fit for total conductivity calculated using Eq. (3), along with individual contributions from each conduction mechanism. Values for the model parameters are given in Table I. Specific details for each of the four materials are discussed in separate sections below.

The process to determine the fitting coefficients is now described. First, σ_{DC} is determined by examining average currents and voltages near the end of the run. This can be complicated if the measurements were not run long enough for the sample to come to equilibrium, $\tau_{exp} < \tau_{eq}$, as is the case for LDPE in Fig. 2(a). Complications also arise if there are significant changes in σ_{DC} due to diurnal changes in temperature in the lab, illustrated for LDPE and BOPP in Figs. 2(a) and 6(b), respectively. If $\left[\frac{d\sigma_{DC}(T)}{dT}\right] \cdot \Delta T_{diurnal} \ll \Delta\sigma_{DC}$, these fluctuations are not seen; however, this effect is observed for all materials even at very low conductivities. It is also difficult if the dark conductivity falls below the instrumental resolution, $\sigma_{DC} < \Delta\sigma_{res}$, as is the case for BOPP in Fig. 6. Several diurnal averages of σ_{DC} are taken at constant sample temperatures near the end of the run; if these values agree, the equilibrium dark conductivity can be determined.

Once σ_{DC} has been determined, this value is subtracted from the data, better exposing the dispersive and transitive behavior in the residual conductivity [see, *e.g.,* Fig. 3(b)]. Finding $\tau_{transit}$ follows easily for each material, as the time corresponding to a distinct change in slope in the residual conductivity on a log-log plot is evident. Note, it is still possible for PI to determine the kink at the longer $\tau_{transit} = 40$ hr, despite the low transitive conductivity, $\sigma_{trans}(\tau_{transit})$, of $1.7x10^{-20}(\Omega \cdot cm)^{-1}$, ~25% above σ_{DC}. Conversely for LDPE, $\sigma_{trans}(\tau_{transit})$ is over an order of magnitude higher at $5x10^{-19}(\Omega \cdot cm)^{-1}$, ~60% of its high σ_{DC} value of $8.3x10^{-19}(\Omega \cdot cm)^{-1} \pm 4\%$.

Once $\tau_{transit}$ is established, values for the parameters σ^0_{disp}, σ^0_{trans}, and α are found for the best fit in the long time residual conductivity. Since dispersive transport theory considers α as an intrinsic material quality characterizing the energy distribution of localized states, efforts are made to keep α the same for both dispersive and transitive conductivities.

With the time-dependent dispersive and transitive conductivity fits determined, they are also subtracted from the total conductivity, allowing the remaining residual data to be described by a polarization contribution [see, *e.g.,* Fig. 4(b)].

The time when the sample reaches equilibrium, τ_{eq}, is when the last time-varying component of conductivity, the transitive contribution, becomes negligible. Quantitatively, this is defined here as when the transitive conductivity equals the standard deviation of σ_{DC}, $\Delta\sigma_{dc}$; that is, τ_{eq} occurs when $(\sigma^0_{trans} \cdot {\tau_{eq}}^{-(1+\alpha)}) = \Delta\sigma_{DC}$. For example, PEEK has an uncertainty of $\Delta\sigma_{DC} = 3x10^{-21}\ (\Omega \cdot cm)^{-1}$, where as seen in Fig. 5(a) the transitive conductivity reaches this value at ~64 hrs. When PEEK—with its low σ_{DC}—is in equilibrium by this definition, the transitive component accounts for ~30% of the total conductivity at τ_{eq}. For materials with a higher σ_{DC} such as LDPE (see Table I), $\Delta\sigma_{DC}$ has a lower fractional uncertainty associated with it, and hence the transitive conductivity has a smaller contribution of ~4% to the total conductivity at τ_{eq}.

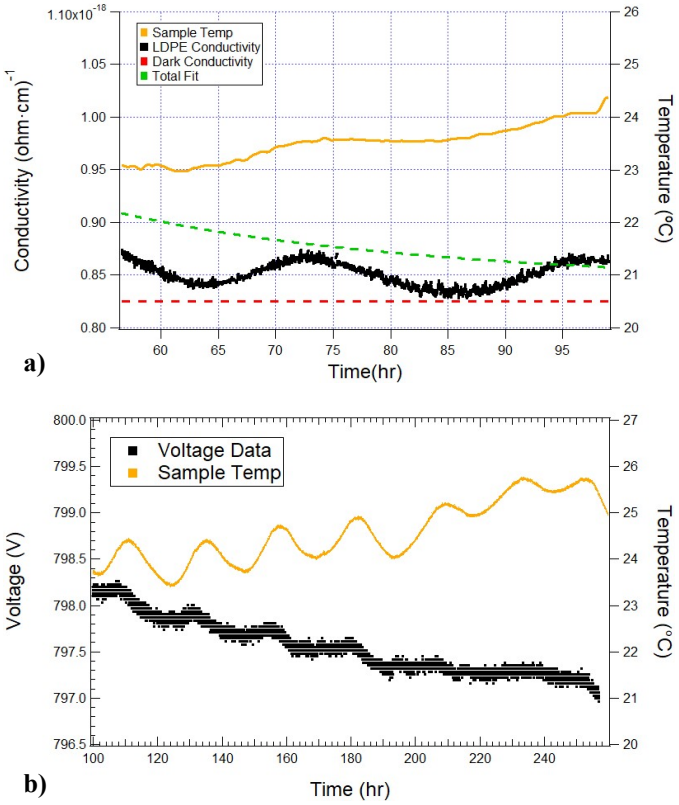

Fig. 2: (a) Linear plot of the temperature dependence of conductivity data (dots) and sample temperature (yellow curve) at long experimental times for LDPE. The total (green) and σ_{DC} (red) conductivity fits are shown, illustrating that the conductivity data has not yet reached the dark conductivity value. (b) Applied voltage versus ambient temperature for BOPP, showing the diurnal changes in voltage, along with the slow dissipation of potential of 1.4 V over 220 hours.

Temperature and conductivity data of LDPE and PEEK are plotted in Figs. 2(a) and 5(b) and 5(c), respectively, with temperature and current results shown in Fig. 6(b) for BOPP. In each case (and also PI), sample temperature data has distinct diurnal fluctuations on the order of ±0.3 K over 24 h, which result from the room's heating cycle. The dark conductivity clearly rises and falls with these temperature fluctuations. The temperature coefficient of dark conductivity, σ^0_T, can be estimated as the ratio of conductivity change to temperature change over 12 hr cycles, as listed in Table I. BOPP has the largest response to temperature, and although BOPP's temperature coefficient is 2 orders of magnitude smaller than LDPE, the ratio of σ^0_T to σ_{DC} is larger; PI and PEEK have similar σ^0_T values. Due to the large reaction to temperature that BOPP sees, more data is needed to retrieve better values for σ^0_T. Temperature coefficients listed in Table I are calculated in small temperature intervals of ~0.5 K, and also where temperature inflections are occurring. Figure 5(b) shows a

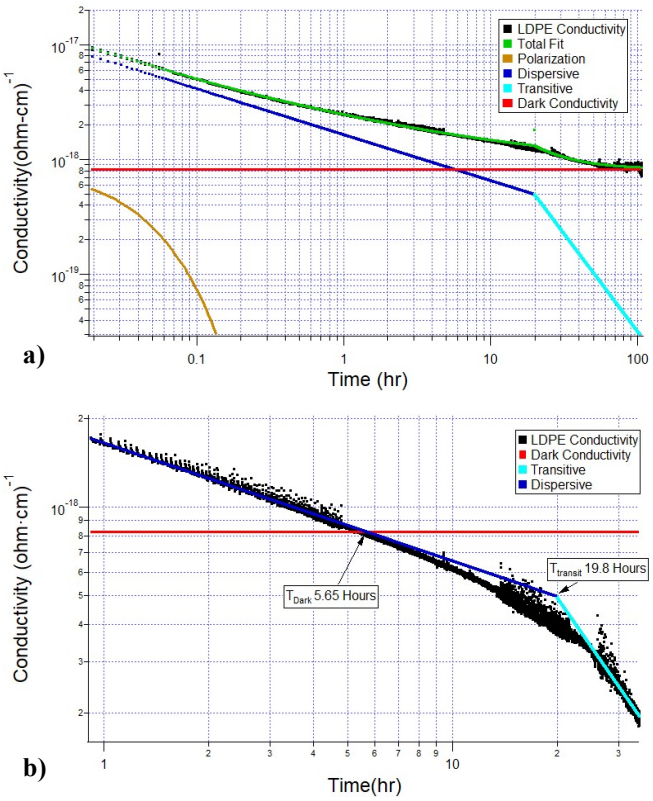

Fig. 3: Time-dependent Conductivity for LDPE. (a) Log-log plot of conductivity data over the full experiment duration with total fit using Eq. (3) and its components. (b) Log-log plot of residual conductivity data near $\tau_{transit}$, with σ_{DC} subtracted, along with dispersive and transitive conductivity fit components. This shows the kink at $\tau_{transit}$ at 19.8 hr, along with the dispersive component reaching the σ_{DC} value at ~5.7 hr.

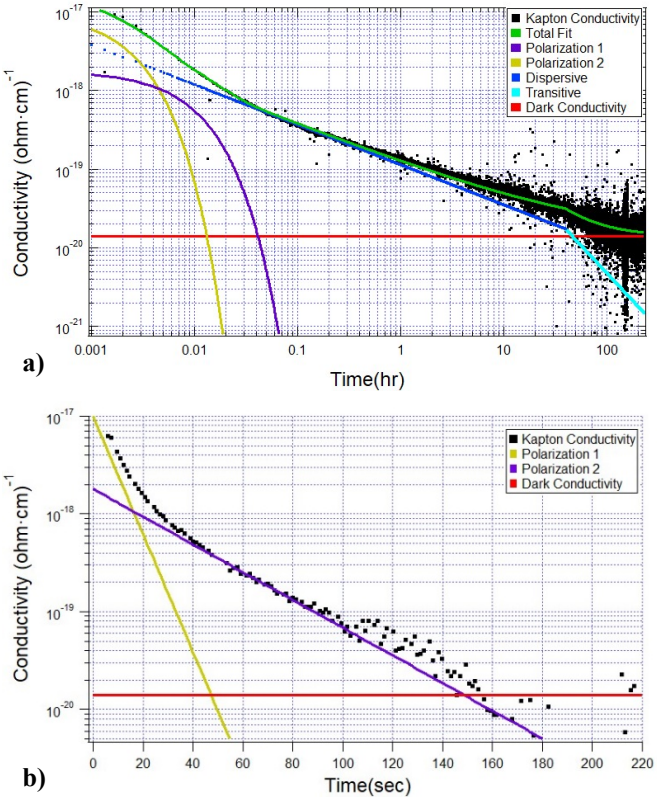

Fig. 4: Time-dependent conductivity for PI. (a) Log-log plot of conductivity data over the full experiment duration, along with the total fit using Eq. (3) and its components. This shows the kink at $\tau_{transit}$ at ~40 hr, along with the transitive component reaching the σ_{DC} value at ~47.2 hr. Note that two polarization components are included. (b) log-linear plot of conductivity data at early times (note scale in seconds). σ_{disp}, σ_{trans}, and σ_{DC} components have been subtracted from the data, leaving only the contributions from polarization. Fitting components for σ_{P1}, σ_{P2}, and σ_{DC} components are shown, where it can be seen that two polarization terms are needed to fit the two slopes of remaining data.

PEEK data set taken over a larger temperature window with a gradual cooling rate of ~2 K/hr. A linear fit has a slope of about 2 to 4 times larger than the value for σ_T^0 given in Table I, making values in Table I a reasonable estimate. Future data over wider temperature ranges above and below room temperature and in both heating and cooling modes (see for example ref. [26]) are needed to understand its relation to σ_{DC} in both hot and cold, and heating and cooling regimes to determine σ_T^0 more precisely.

It is testament to the resolution of the conductivity data that for LDPE the effects of a small decreasing $\sigma_{trans}(t)$ can be extrapolated to show it counterbalances increases in σ_{DC} due to overall increasing temperature [see Fig. 2(a)]. Likewise, for PEEK the effects of small (but still decreasing) $\sigma_{trans}(t)$, extrapolated to only 10% of σ_{DC}, can be effectively removed from any changes in σ_{DC} due to in temperature trends [see Fig. 5(c)].

The following subsections now present the results of long time scale conductivity measurements of the four polymeric materials.

A. Low-Density Polyethylene

Time-dependent conductivity data for LDPE are shown in Fig. 3(a) as a log-log plot of conductivity data over the full experiment duration of 107 hr. LDPE CVC data were acquired using an applied voltage of ~420 V, or ~17 MV/m (~9% of nominal breakdown voltage for vacuum baked samples [22]).

Fits to the total conductivity using Eq. (3) and its components are also shown in Fig. 3(a), with fitting parameters listed in Table I. The value of conductivity after only 1 hr of applied voltage at 23.9 °C, $\sigma(t = 1\ hr) = 2.6x10^{-19}(\Omega \cdot cm)^{-1}$, is in very good agreement with previous measurements on similar LDPE samples of $\sigma(t = 1\ hr) = 4x10^{-19}(\Omega \cdot cm)^{-1}$ at the same temperature and applied field [26].

The LDPE polarization amplitude, σ_P^o, is about the same as σ_{DC}, and is about half the magnitude of that for PEEK, BOPP, and the second σ_P^0 of PI. This is expected for a relatively non-polar structure like $[H\text{-}C\text{-}H]_n$. With the polarization decay time of 144 s, the polarization contribution falls below the σ_{DC} value at just ~12 s, and below $\Delta\sigma_{DC}$ at ~490 s.

Figure 3(b) shows a log-log plot of residual conductivity data near $\tau_{transit}$ with σ_{DC} subtracted, along with dispersive and transitive conductivity component fits. This highlights the dispersive transport kink at $\tau_{transit} = 19.8$ hrs, and when the dispersive component reaches and falls below σ_{DC} at ~5.7 hr. At $\tau_{transit}$ the transitive contribution has fallen to

$5x10^{-19}(\Omega \cdot cm)^{-1}$, ~60% of σ_{dc}. Values for α for the dispersive and transitive regimes, $\alpha_{disp} = 0.6$ and $\alpha_{Trans} = 0.7$, are in good agreement with the average value $\bar{\alpha} = 0.65 \pm 0.5$ in Table I and of α_{disp}=0.62 [26] and $\alpha_{disp} > 0.6$ [23] from previous studies.

The temperature coefficient of dark conductivity, $\sigma_T^0 = \sim 8x10^{-20} \frac{(ohm \cdot cm)^{-1}}{K}$ can be estimated as the ratio of conductivity change to temperature change over a 12 hr cycle, as listed in Table I. This is in reasonable agreement with a previous measurement of $\sim 2x10^{-19} \frac{(ohm \cdot cm)^{-1}}{K}$ [26].

B. Polyimide

Time-dependent conductivity data for PI are plotted in Fig. 4. PI CVC data were acquired using an applied voltage of ~800 V or ~32 MV/m (~11% of nominal breakdown voltage for vacuum baked samples [22]). Figure 4(a) shows the results of the entire run as a log-log plot of conductivity over the full experiment duration with the model and its constituents. This run lasted 231 hrs, significantly longer than for LDPE, although it reached equilibrium at 154 hrs, with $\sigma_{DC} = 1.5 \pm 0.3 \times 10^{-20}\ (\Omega \cdot \mathrm{cm})^{-1}$. Significant noise is seen at the end of this run as the measured current approaches the limit of the instrumentation, $\Delta\sigma_{res}$. This produces some ambiguity in determining $t_{transit}$, which was estimated as ~40 hrs. In the case of PI, it is the transitive contribution that reduces to σ_{DC}, occurring at 44.8 hrs or about 29% of τ_{eq}. PI had the largest discrepancy among α values, with α_{disp} and α_{trans} having values of 0.49 and 0.3, respectively; $\bar{\alpha} = 0.4 \pm 0.1$ is about 38% percent less than the value for LDPE.

The magnitude of the polarization component is larger for PI than for LDPE or other samples, and up to three orders of magnitude larger than σ_{DC} for PI during the initial seconds. There are two polarization contributions evident in the log-linear plot of conductivity data at early times, Fig. 4(b), with σ_{DC} and the dispersive contribution subtracted from the raw conductivity data to determine the attributes of the polarization mechanisms. The first polarization component has a large magnitude of $1.0x10^{-17}(\Omega \cdot cm)^{-1}$, but with a rapid decay time of 7.2 s. The second polarization component has a magnitude similar to those of all the other samples of $\sim 1x10^{-18}(\Omega \cdot cm)^{-1}$, and a decay time of 30.6 s, with it matching σ_{DC} at 144 secs.

Poly-Ether Ether Ketone

Time-dependent conductivity data for PEEK are shown in Fig. 5(a) as a log-log plot of conductivity data over the full experiment duration of 142 hrs. PEEK CVC data were acquired using an applied voltage of ~800 V or ~32 MV/m (~16% of nominal breakdown voltage for vacuum baked samples [22]).

PEEK has a low σ_{DC} value of $(7 \pm 3)x10^{-21}(\Omega \cdot cm)^{-1}$, three orders of magnitude less than σ_P^o and σ_{trans}^o. Even at extended time scales, the dispersive component is the main contributor to the total conductivity due to the low σ_{DC}. PEEK has the most consistent values of α_{disp}=0.45 and $\alpha_{trans} = 0.44$ of the four polymers, with $\bar{\alpha} = 0.445 \pm 0.005$. The polarization drops below σ_{DC} in 63 s, which is similar to the polarizations of PI on the order of minutes. For PEEK, $\tau_{transit} = 20$ hr; PEEK's transitive contribution falls below σ_{DC} at 35.6 hours, about 56% of the equilibrium time, but is comparable to PI, which has a similar $\bar{\alpha}$. Equilibrium is reached at 64.1 hrs, the most rapid of the four polymers.

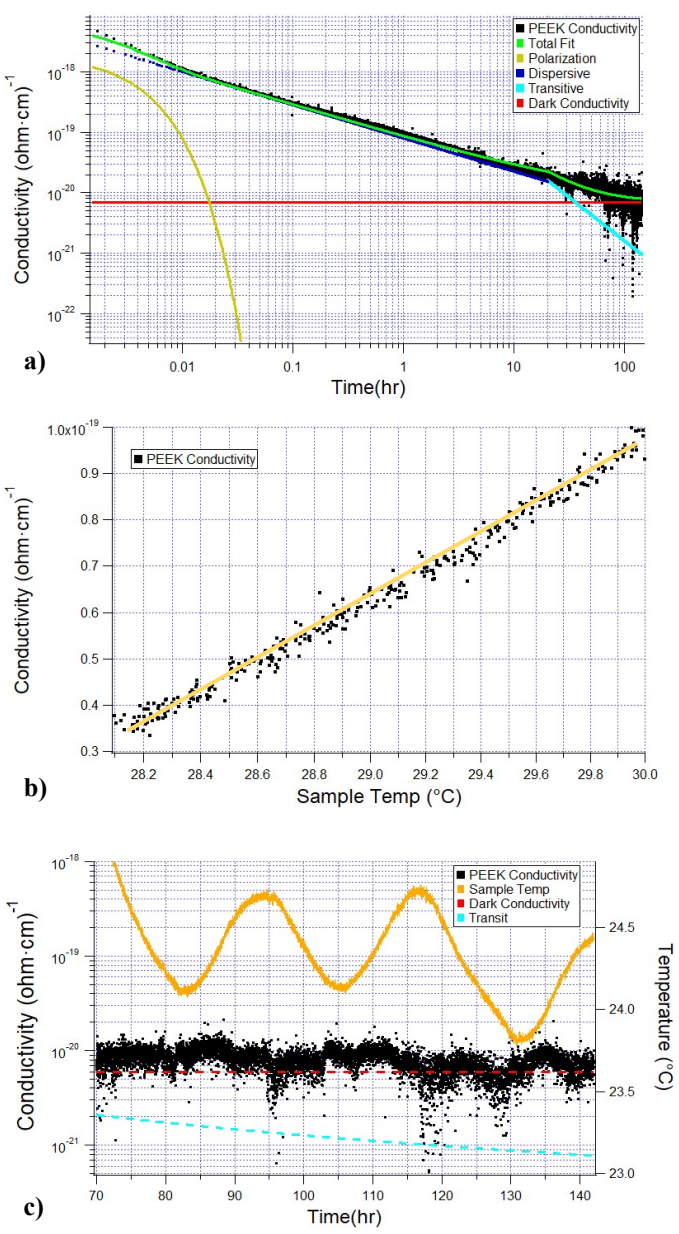

Fig. 5: Time-dependent Conductivity for PEEK. (a) Log-log plot of conductivity data over the full experiment duration with total fit using Eq. (3) and its components. (b) Equilibrium conductivity as a function of sample temperature, taken during a cooling rate of ~2 K/hr on a separate run. A linear fit is shown in yellow with a slope of $\sim 4x10^{-20} \frac{(ohm \cdot cm)^{-1}}{K}$. (c) Semi-log plot of the temperature dependence of conductivity data, showing a diminishing transitive contribution extrapolated to 10% of σ_{DC}.

C. Polypropylene

Time-dependent conductivity data for BOPP are shown in Fig. 6(a) as a log-log plot of conductivity data over the full

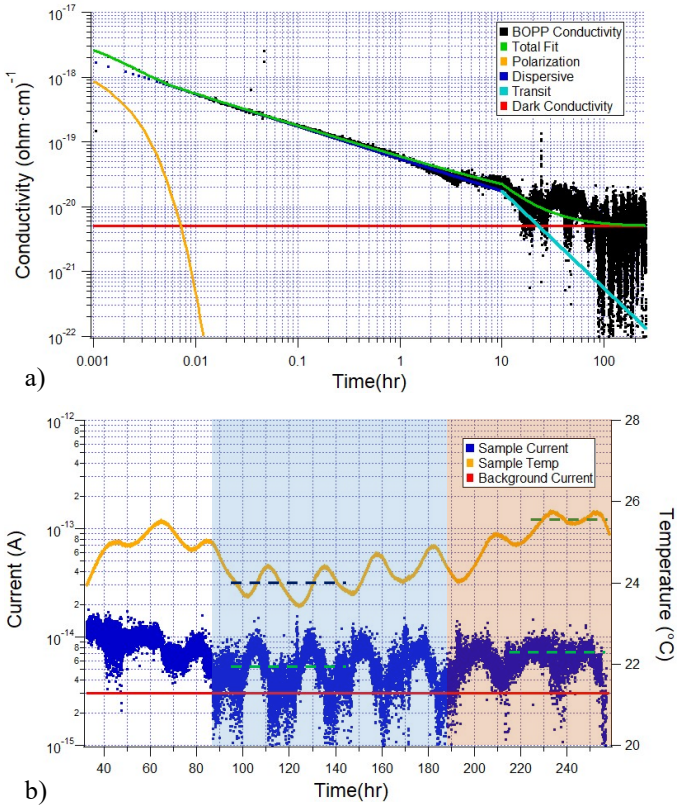

Fig. 6: Time-dependent conductivity for BOPP. (a) Log-log plot of conductivity data over the full experiment duration fit using Eq. (3). (b) Semi-log plot of the temperature dependence of current data, along with the background current which sets the limit of measurement. The blue shaded region shows where the measured current reaches the limit and the diurnal temperature changes push the current below the background level. The average value for the conductivity at this plateau is less than $\Delta\sigma_{res}$, and thus cannot be reported. The red shaded area indicates the current data coming above the background as a result of overall temperature increase, with the average conductivity taken between 225-255 hrs used for σ_{DC}.

experiment duration of 257 hrs. BOPP CVC data were acquired using an applied voltage of ~800 V or ~32 MV/m (~9% of nominal breakdown voltage for vacuum baked samples [22]). Fitting BOPP data to the conductivity with Eq. (3) cannot be done as reliably, due to the heightened sensitivity of this material to temperature fluctuations. Additional tests need to be made, using possible conditioning of samples or temperature management to achieve steadier data. Figure 6(a) shows the best attempt to fit the data with Eq. (3). Parameters for DC, polarization and dispersion are fit reasonably well, while the transit time and transitive attributions get masked in the temperature fluctuations.

Figure 6(b) shows current data collected of BOPP on a log-linear plot, along with the sample temperature; this emphasizes the diurnal temperature fluctuations influence on the collected data. The data have a considerable response to changes in temperature, that is exacerbated when the current data reach the electrometer's inherent background current level (red horizontal line), shown in the blue shaded region in Fig. 6(b), occurring between ~86 to ~183 hrs. When the conductivity is calculated, the background current is removed from the current data, heightening this effect and producing the results shown in Fig. 6(a), where the red line shows $\sigma_{DC} = (5 \pm 3)x10^{-21}(\Omega \cdot cm)^{-1}$ at 25.7 °C, which is very similar to the conductivity resolution limit of $\Delta\sigma_{res} = 4.9\,x10^{-21}(\Omega \cdot cm)^{-1}$ determined by the background current level. The overall temperature increase in the red shaded region was necessary to calculate a DC value for BOPP above the resolution of our instrumentation. Taking a conductivity average over a period of data from 95-145 hours gives $\sigma_{DC} = (3 \pm 4)x10^{-21}(\Omega \cdot cm)^{-1}$ at 25.7 °C, and thus the best reported value for σ_{DC} is less than or equal to the background conductivity value at this time interval at the reported temperature, and cannot report an equilibrium time.

VI. Conclusions

The CVC test apparatus, and in particular the use of very stable battery voltage supplies [13], is found to provide high resolution measurements of the time-dependent conductivity of HDIM. The lower limit of conductivity measured with the instrument is $\Delta\sigma_{res} = 2x10^{-21}(\Omega \cdot \mathrm{cm})^{-1}$, which corresponds to τ_{decay} of >1 yr, for typical values of experimental parameters used here as set by the precision in the current measurements of ~1 fA. When samples reach equilibrium currents, signal averaging of measurements over 10^3 s can typically reduce the precision to $\sim 1 \times 10^{-16}$ A and $\Delta\sigma_{res} = 2x10^{-22}\ (\Omega \cdot \mathrm{cm})^{-1}$, which corresponds to τ_{decay} of >1 decade. Use of an improved electrometer with ~0.1 fA resolution is also expected to extend $\Delta\sigma_{res}$ an order of magnitude.

The time-dependent conductivities and associated physical parameters have been determined for each of four common polymeric materials used in space applications. Ranking of σ_{DC} from highest to lowest is LDPE, PI, PEEK, and BOPP, although the relative contributions from the different macroscopic conduction mechanisms exhibit different ordering. In general, these results are consistent with expectations and the limited available results from previous studies. Measurements are in progress to study other polymeric and glass/ceramic HDIM. Operationally, determining smaller conductivities and longer decay times is not necessary for all but the very longest duration space missions or other applications. In addition, the enhanced sensitivity of the CVC apparatus allows study of new aspects of the transport process and materials characteristics.

Results using the CVC method for time-dependent conductivity measured over more than five orders of magnitude in time are found to be described very well by the macroscopic conductivity model for the CVC method presented in Eq. (3), which includes terms for polarization, dispersive and dark current conductivities. We can draw some conclusions about the time constants describing time-dependent conductivity from our measured results. First, the general order of the time constants listed in Eq. (4) and summarized in Table I was confirmed for all four materials, with a few minor exceptions.

Exponential decay over short time scales of 10^0 s to 10^3 s is attributed to polarization effects. These polarization terms are attributed to either interfacial or electrode polarization mechanisms found in semi-crystalline polymers [27] based on their long decay times, rather than from either electronic or atomic polarizations that occur on much shorter time scales [28]. LDPE's σ_P^o has a one to two orders of magnitude lower

TABLE I
SUMMARY OF CONDUCTIVITY MODEL PARAMETERS FOR POLYMER SAMPLES

Symbol	Quantity	Units	Low Density Polyethylene	Polyimide	Polyether Ether Ketone	Poly-propylene
σ_P^0	Polarization Amplitude	$(\Omega \cdot cm)^{-1}$	$9x10^{-19}$	1: $1.0x10^{-17}$ 2: $1.8x10^{-18}$	$2x10^{-18}$	$2x10^{-18}$
σ_{disp}^0	Dispersive Amplitude	$(\Omega \cdot cm)^{-1}$	$1.7x10^{-18}$	$1.1x10^{-19}$	$8.0x10^{-20}$	$5.5x10^{-20}$
σ_{trans}^0	Transitive Amplitude	$(\Omega \cdot cm)^{-1}$	$8.0x10^{-17}$	$2.1x10^{-18}$	$1.2x10^{-18}$	-
σ_{DC}	Dark Conductivity	$(\Omega \cdot cm)^{-1}$	$(8.3 \pm 0.3)x10^{-19}$ @ 23.9 ℃	$(1.5 \pm 0.3)x10^{-20}$ @ 25.6 ℃	$(7 \pm 3)x10^{-21}$ @ 24.2℃	$(5 \pm 3)x10^{-21}$ @ 25.7℃
$\Delta\sigma_{DC}$	Dark Conductivity Std. Deviation	$(\Omega \cdot cm)^{-1}$	$3x10^{-20}$	$3x10^{-21}$	$3x10^{-21}$	$3x10^{-21}$
$\frac{\sigma_{trans}^0}{\sigma_{disp}^0}$	Transit-Dispersion Ratio	*(unitless)*	48	18	15	-
σ_T^0	Conductivity Temp. Coefficient	$\frac{(\Omega \cdot cm)^{-1}}{K}$	$8x10^{-20}$	$2x10^{-21}$	$4x10^{-20}$	$7x10^{-22}$
τ_P	Polarization Decay Time	*s*	144.0	1: 7.2 2: 30.6	11.1	4.3
$\tau_{transit}$	Transit Time	*days*	0.83	1.7	0.83	-
$\bar{\alpha}$	Dispersion Parameters	*(unitless)*	0.65 ± 0.05	0.4 ± 0.1	0.445 ± 0.005	0.5
α_{disp}			0.6	0.49	0.45	0.5
α_{trans}			0.7	0.3	0.44	-
τ_{decay}	Decay Time	*days*	2.8 ($\epsilon_r = 2.3$)	232 ($\epsilon_r = 3.4$)	476 ($\epsilon_r = 3.5$)	492 ($\epsilon_r = 2.4$)
τ_{eq}	Equilibrium Time	*days*	4.3	6.4	2.7	-
$\frac{\tau_{decay}}{\tau_{eq}}$	Decay-Equilibrium Ratio	*(unitless)*	0.63	36	159	-
$\frac{\tau_{transit}}{\tau_{eq}}$	Transit-Equilibrium Ratio	*(unitless)*	0.19	0.27	0.24	-
τ_{exp}	Experiment Duration	*days*	4.5	9.6	5.9	10.7

value than the other three polymeric materials, which we attribute to the non-polar nature of LDPE. Further, LDPE has an order of magnitude longer τ_P than those observed for the other polymers; this suggests that the small polarization term observed for LDPE might be attributable to significant rearrangement of the LDPE polymer chains, in contrast to the other polymers whose chain motion is more sterically inhibited due to more cross-linking and larger side-structures on their polymer chains. The instrumentation is being extended to include faster current measurements, up to two orders of magnitude faster or ~10^{-2} s, for higher currents observed in the initial 10^2 s; this will allow consistent measurements of instrumentation and charge injection behavior through τ_Q [9], as well as faster polarization terms [8].

The two power law time-dependent regions for dispersive and transitive conductivity, the associated kink at $\tau_{transit}$, and the relative agreement between α_{disp} and α_{trans} confirm the predictions by Scher and Montroll based on hopping conductivity and multiple trapping models for highly disordered materials. Indeed, studies with this CVC apparatus on polymeric HDIM have remarkably extended the striking scaling characteristic of Scher-Montroll theory over more than eight orders of magnitude in time from 10^{-3} s < $\tau_{transit}$ < 10^1 s observed for amorphous semiconductors [3,11] to $\tau_{transit} \gtrsim 10^5$ s for HDIM. The observed order of α and τ_P are the same for the four materials. This is consistent with the conjecture that large τ_P is attributable to significant rearrangement of the LDPE polymer chains which could lead to a higher degree of microscopic structural disorder, a broader distribution of defect state energies, and a larger value of α.

Each material is found to reach (or at least approach) a well-defined constant dark current conductivity at long times, although the enhanced sensitivity of the CVC tests allows subtle changes in σ_{DC} due to temperature and voltage fluctuations over 10^3 s time scales to be observed and quantified. A definition has been proposed for equilibration time for CVC measurements, τ_{eq}, after which conductivity reaches a constant σ_{DC}. Although this definition of τ_{eq} depends on instrumentation

properties through $\Delta\sigma_{res}$, it still seems to provide a better estimate of equilibrium time scales for CVC measurements than τ_{decay} which seems more applicable to CSC measurements. The ratio [$\tau_{transit}$ / τ_{eq}] =0.23±15% is very consistent, whereas the ratio [τ_{decay} / τ_{eq}] varies more than two orders of magnitude for the four polymers due to the added permittivity influence. The experiment durations here, τ_{exp}, all exceed τ_{eq} but do not reach τ_{decay}; LDPE experiments are the only exception. Note that the ratio [$\sigma^0_{disp}/\sigma^0_{trans}$] is linearly correlated with the ratio [$\tau_{transit}$/ τ_{eq}], with a proportionality constant 5.6 ± 1.6 to within the variations of these ratios amongst the four polymers; this is reasonable, as τ_{eq} is related to the ratio of $\Delta\sigma_{res}$ to σ^0_{trans}. By contrast, σ_{DC} is not found to be correlated with σ^o_P, σ^0_{disp}, or σ^0_{trans}; this lack of correlation is consistent with the proposition that polarization, dispersive transport and dark conductivity are independent conduction mechanisms.

Measurements of equilibrium σ_{DC} subject to small diurnal fluctuations in temperature as small as ±0.5 K have been used to determine values of σ^0_T, which are found to agree with limited results determined by other methods. Further studies will also investigate the temperature dependent dark current conductivity; these will include measurements where the temperature of materials which have reached equilibrium σ_{DC} are slowly cycled up and down to determine T-dependent $\sigma^0_T(T)$ [8]. Preliminary studies of the field-enhanced conductivity [9] can now be extended to fields well below 10 % of the breakdown field strength, with the enhanced sensitivity of the CVC apparatus.

VII. Acknowledgment

We acknowledge invaluable assistance with instrumentation and data acquisition from current and previous members of the Utah State University Materials Physics Group, including Phillip Lundgreen, Ryan Hoffmann, Steven Hart, Jerilyn Brunson, and Anthony Thomas.

VIII. References

[1] D. Hastings, and H. Garrett, *Spacecraft-environment Interactions*, Cambridge University Press, 1996.

[2] D.C. Ferguson, "New Frontiers in Spacecraft Charging." *IEEE Trans. Plasma Sci.*, vol. 40, no.2, pp. 139-143, 2012.

[3] R. Zallen, *The Physics of Amorphous Solids*, New York, NY, USA: John Wiley & Sons Inc., 1998.

[4] A.M. Sim, JR Dennison, "Comprehensive Theoretical Framework for Modeling Diverse Electron Transport Experiments in Parallel Plate Geometries," 5th AIAA Atmospheric and Space Environ. Conf., San Diego, CA, June 24-27, 2013.

[5] C.C. Reed, R. Briët, and M. Begert, "ESD Detection, Location and Mitigation, and Why they are Important for Satellite Development." 13th Spacecraft Charging Tech. Conf., Pasadena, CA, June, 2014.

[6] H.B. Garret, A.C. Whittlesey, "Spacecraft Charging, An Update." *IEEE Trans. Plasma Sci.*, vol. 28, no. 6, pp. 2017-2028, 2000.

[7] "Avoiding problems caused by spacecraft on-orbit internal charging effects," NASA-HDBK-4002, NASA, 1998.

[8] J. Dekany, JR Dennison, A.M. Sim, J. Brunson, "Electron Transport Models and Precision Measurements with the Constant Voltage Conductivity Method." *IEEE Trans. Plasma Sci.*, vol. 41, no. 12, pp.3565-3576, 2013.

[9] J. Brunson "Hopping Conductivity and Charge Transport in Low Density Polyethylene," Ph.D. Dissertation, Utah State Univ., Logan, UT, 2010

[10] S. Baranovskii, O. Rubel, *Springer Handbook of Electronic and Photonic Materials*, Springer International Publishing, 2017.

[11] H. Scher, E.W. Montroll, "Anomalous Transit-Time Dispersion in Amorphous Solids." *Phys. Rev. B*, vol. 12, no. 6, pp. 2455-2477, 1975.

[12] ASTM D 257-99, "Standard Test Methods for DC Resistance or Conductance of Insulating Materials" *Am. Soc. for Testing and Materials*, West Conshohocken, PA 19428, 1999.

[13] David King, "Constant Voltage Conductivity with Temperature and Radiation Effects," Senior Thesis, Utah State University, Logan, UT, May 2017.

[14] ASTM, "Standard Specification for Polymeric Resin Film for Electrical Insulation and Dielectric Applications," vol. D5213-12, ed, 2012.

[15] "Material Information-Polyethylene Low Density LDPE," Goodfellow, Ed., ed. Devon, PA, 2006.

[16] H. J. Wintle, "Conduction Processes in Polymers," in *Engineering Dielectrics-Volume IIA: Electrical Properties of Solid Insulating Materials: Molecular Structure and Electrical Behavior*. vol. IIA, R. Bartnikas, Ed., ed Philadelphia, PA: American Society for Testing and Materials, 1983.

[17] Prasanna V. Swaminathan, "Measurement of charge decay time and resistivity of spacecraft insulators," M.S. Thesis, Utah State Univ., Logan, UT, 2004.

[18] A. Peacock, *Handbook of polyethylene: structures: properties, and applications*: CRC Press, 2000.

[19] "DuPont Kapton HN polyimide film, H-38479, Bulletin GS-96-7,," vol. document K-15345-1, DuPont, Ed., ed. Circleville, OH, USA, 2011.

[20] "Standard Price List for Polyetheretherketone," Goodfellow, Ed., ed. Coraopolis, PA, 2016.

[21] "Standard Price List for Polypropylene," Goodfellow, Ed., ed. Coraopolis, PA, 2017.

[22] A. Andersen, "The Role of Recoverable and Irrecoverable Defects in DC Electrical Aging of Highly Disordered Insulating Materials," Ph.D Dissertation, Utah State Univ., Logan, UT, 2018.

[23] V. Adamec and J. H. Calderwood, "On the determination of electrical conductivity in polyethylene," *J. Phys. D: Appl. Phys.*, 14, 1487-1494, 1981

[24] ASTM, "Standard Test Method for Electric Breakdown Voltage and Dielectric Strength of Solid Electrical Insulating Materials at Commercial Power Frequencies," vol. D149-97a, ed, 2004.

[25] C. Amsler, et al, "Review of Particle Physics," *Phys. Lett. B*, vol. 667, 1, 2008.

[26] J.R. Dennison and J. Brunson, "Temperature and Electric Field Dependence of Conduction in Low-Density Polyethylene," *IEEE Trans. Plasma Sci*., vol. 36, no. 5, 2246-2252, 2008.

[27] H. Lu, X. Zhang, H. Zhang, "Influence of the Relaxation Maxwell-Wagner-Sillars polarization and dc Conductivity on the Dielectric Behaviors of Nylon 1010," *J. Appl. Phys.* vol. 100, no. 5, 2006.

[28] J.C. Anderson, K.D. Leaver, R.D. Rawlings, J.M. Alexander, *Materials Science*, New York, NY, USA: Chapman and Hall, 1990.